Leaching characteristics of naturally derived toxic elements in the alluvial marine clay layer beneath Osaka Plain, Japan: implications for the reuse of excavated soils

Leaching characteristics of naturally derived toxic elements in the alluvial marine clay layer beneath Osaka Plain, Japan: implications for the reuse of excavated soils

Hiroko Ito, Harue Masuda, Akihiko Oshima

Ito, H., Masuda, H. & Oshima, A. Leaching characteristics of naturally derived toxic elements in the alluvial marine clay layer beneath Osaka Plain, Japan: implications for the reuse of excavated soils. *Environmental Earth Sciences*. 78, 589 (2019). Doi:10.1007/s12665-019-8595-3

Title:

Leaching characteristics of naturally derived toxic elements in the alluvial marine clay layer beneath Osaka Plain, Japan: implications for the reuse of excavated soils

Authors:

Hiroko Ito[1, 2*], Harue Masuda[2], and Akihiko Oshima[3]

Institution Address:

[1] Geo-Research Institute, 6F, Kokuminkaikan Sumitomoseimei Bldg. 2-1-2, Otemae, Chuo-ku, Osaka 540-0008, Japan
e-mail: ito@geor.or.jp

[2] Department of Geosciences, Osaka City University, 3-3-138, Sugimoto, Sumiyoshi-ku, Osaka 558-8585, Japan
e-mail: harue@sci.osaka-cu.ac.jp

[3] Department of Urban geoengineering, Osaka City University, 3-3-138, Sugimoto, Sumiyoshi-ku, Osaka 558-8585, Japan
e-mail: oshima@civil.eng.osaka-cu.ac.jp

* Corresponding author: e-mail: ito@geor.or.jp tel:+81-6-6941-8833
ORCID: 0000-0001-5417-0775

Abstract

The risks of contamination by naturally derived toxic elements must be assessed to achieve a sustainable geo-environment when promoting the utilization of excavated surplus soils. To estimate the controlling factors and risks of groundwater pollution associated with the application of recycled excavated surplus soils, we analyzed the bulk concentrations and sequentially extracted fractions of major and toxic elements, and compared these results to the water-soluble concentrations extracted by the simple batch leaching test required by Japanese regulations.

Our results showed that toxic elements such as B and Pb were concentrated in the marine clay layer Ma13, especially where clay fractions were dominant. Arsenic was easy to be released from the sediments under changing redox conditions, especially in transitional sandy silt layers. We demonstrate that the 0.45 μm filter required by Japanese regulations does not efficiently remove colloidal particles, which affects the reproducibility of batch leaching tests, especially for Pb, and the relative indices of metal mobility suggest that the long-term risk of groundwater contamination resulting from the reuse of excavated surplus soils may not be estimated accurately only by the simple batch leaching test. The change of redox conditions that occurs upon the exposure of excavated surplus soils to the air must be considered to fully evaluate the risk of toxic element mobilization.

Key Words

host phases of toxic elements, excavated surplus soils, boron, arsenic, lead

1. Introduction

Naturally derived toxic elements are a major issue in handling excavated surplus soils in Japan. Under conventional law, excavated soils with naturally derived toxic element contents exceeding soil environmental standards had to be treated at a final waste disposal site. However, the "Amendment to the Soil Contamination Countermeasures Act" was promulgated in May 2017 (Japanese Ministry of the Environment 2017 a) to streamline regulations and reduce the risk of contamination when using excavated surplus soil. Risk assessments have and will be continuously performed by the Ministry of the Environment to enforce the revised law until May 2019. One of the most important issues when streamlining the regulations was developing methods and procedures for the effective utilization of naturally derived contaminated soils (Japanese Ministry of the Environment 2017 b).

According to the law, contaminated areas must be specified based on analytical results of simple batch and acid leaching tests based on Environmental Agency notifications nos. 18 and 19 (Japanese Ministry of the Environment 2003 a-b, respectively). These methods were established based on assessments of the health risk to the human body, assuming that soil pollutants are ingested as dissolved matter in groundwater and/or as soil dust. These analyses are generally performed immediately after excavations. However, the long-term risk of groundwater pollution cannot be evaluated by these analyses, because pollutants released during soil excavation are oxidized when exposed to aerobic conditions. Thus, various analytical methods have been proposed for more realistic risk assessments of contaminated soils, including column tests, oxidation tests, serial batch leaching tests, and rainwater exposure tests (Public Works Research Institute et al. 2015).

The alluvial marine clay layer Ma13 is widely distributed and ≥10 m thick beneath the Osaka Plain (KG-NET 2007). This clay layer contains naturally toxic elements such as As, Pb, F, and B (e.g., Ito et al. 2018). The depth to the top of Ma13 is typically <10 m (KG-NET 2007), shallower than the maximum investigation depth specified by "Enforcement Regulation of the Soil Contamination Countermeasures Act" (Japanese Ministry of the Environment 2017 c). To evaluate Ma13 as a possible pollutant source, its geochemical properties immediately after excavation and after replacement for reuse must be clarified. Since most analyses (as required by law) have been performed on soils taken from <10 m depth, the geochemical and physical characteristics of the entire Ma13 layer have not been studied. Here, we performed bulk sediment chemical analyses, sequential extraction tests, and simple batch leaching tests on a sediment core including Ma13 taken from the western part of the Osaka Plain, and discuss the probability of producing pollutants via the dissolution of reused soils.

2. Geological setting of the sampling site

The Osaka Basin (central Japan) developed since 3 Ma (Ichihara ed. 1993) in association with subduction of Philippine Sea Plate beneath the Eurasian Plate. Pliocene to Quaternary sediments reach a maximum thickness of 1,500 m beneath the plain, and more than 20 marine clay layers (deposited in association with cyclic global sea level changes) are intercalated with freshwater sand and gravel layers (Ichihara ed. 1993). Alluvial sediments, including the uppermost marine clay layer Ma13, widely cover the lowlands of the basin (Fig. 1). Ma13 exceeds 10 m thickness and thickens toward the Osaka Bay coast to the west. In this study, we analyzed a sediment core from the western Osaka Basin on the northwest side of the Uemachi Upland, between the Yodo and Okawa rivers. In this core, Ma13 is present at 6–19 m depth from the ground surface (Fig. 2).

3. Analytical methods

3.1 Lithology and physical properties of cored sediments

Undisturbed sediments were drilled using a thin-walled tube sampler with a diameter of 75 mm (JGS1221-2012; Japanese Geotechnical Society 2015). The sediments were pushed out of the samplers and cut into 10-cm-long cores for laboratory engineering soil tests. For chemical analyses, subsamples of the 10-cm core segments were vacuum-packed with a de-oxygenizer immediately after cutting to prevent oxidation.

Lithology was described based on visual observation. To identify the depositional ages of the sediments, a volcanic glass layer was detected by optical microscopic observation, and the refractive indices of the glass fragments were analyzed using a refractometer (RIMS, Kyoto Fission-Track Co., Ltd.) (Danhara et al. 1992) to specify the origin, and thus known depositional age, of the tephra. Physical properties of the sediments (i.e., particle size distribution, natural water content, and loss on ignition, LOI) were determined according to Japanese standard methods (JIS A 1204, 1203, and 1226, respectively; Japanese Industrial Standard Association 2009 a–c).

3.2 Bulk sediment analyses

The sediment samples stored under anaerobic conditions were freeze-dried and powdered using an agate mortar and pestle. Their bulk mineralogies were determined by X-ray powder diffraction (XRD, RAD-1A, Rigaku) with Ni-filtered Cu Kα radiation. The samples were also analyzed by XRD after pretreatment with 1 M HCl to identify chlorite and kaolinite, or ethylene glycol to identify kaolinite and smectite. Major element concentrations (SiO_2, Al_2O_3, Fe_2O_3, MnO, MgO, CaO, Na_2O, and K_2O), were measured by X-ray fluorescence (XRF, VXQ-160S, Shimazu) using the glass bead method, in which sample powders are fused into glass beads with lithium borate at maximum temperatures of 1200 °C. The accuracies of major element analyses were within 4%, confirmed by analysis of Geological Survey of Japan (GSJ) Geochemical Reference sample JB-2, although MnO concentrations were within 5%. Toxic trace element concentrations (i.e., B, As, Pb, Cr, Cd, and Se) were determined by inductively coupled plasma mass spectrometry (ICP-MS, SPQ9700, SII) using the calibration line method after alkaline fusion of the powdered samples and subsequent dissolution in 0.1 M nitric acid. The accuracies of toxic element analyses were within 10%, confirmed by analyses of GSJ Geochemical Reference samples JSd-2 and JSd-3. The obtained results were expressed as the weight of leached elements from the powdered sediments (mg/kg, ppm).

3.3 Sequential chemical extraction experiment (SCEE)

The freeze-dried samples were sequentially reacted with five separate chemical treatments to extract acid-soluble phases, reducible phases, oxidizable phases, insoluble phases, and residual silicates according to the method of Ito et al. (2003), which was modified from that of Thomas et al. (1994) and Wang et al. (1997). This method cannot accurately specify the host phases, but the behaviors of elements with changing environmental redox conditions can be roughly evaluated. The phases were extracted in five steps, as follows.

Step 1: Acid-soluble phases

One gram of each sediment powder was shaken with 20 ml 0.22 M acetic acid (pH adjusted to 5 with ammonium acetate) in a PTFE centrifuge tube for 16 h at room temperature. Then the mixture was centrifuged at 10,000

rpm for 10 min to extract acid-soluble phases (i.e., components weakly adsorbed onto detrital materials or fixed in carbonates). The supernatant solution was diluted by 0.1 M nitric acid to quantify by ICP-MS.

Step 2: Reducible phases

The residual sediment from step 1 was shaken with 20 ml 0.5 M hydroxylammonium chloride (NH_3OHCl, pH adjusted to 2 with HNO_3) for 16 h at room temperature to extract reducible phases mainly fixed in Fe-oxyhydroxides and Mn-oxides. Then the mixture was centrifuged at 10,000 rpm for 10 min to separate the residue. The supernatant solution was diluted by 0.1 M nitric acid to quantify by ICP-MS.

Step 3: Oxidizable phases

The residue from step 2 was heated with 20 ml 0.1 M sodium pyrophosphate for 2 h, then shaken with 10 ml 5 M ammonium acetate (CH_3COONH_4, pH adjusted to 2 with HNO_3) for 16 h at room temperature. This reagent cannot completely decompose sulfide minerals, so the most probable phase dissolved in this step is organic matter. The solution was centrifuged at 10,000 rpm for 10 min to separate the residue. The supernatant solution was diluted by 0.1 M nitric acid to quantify by ICP-MS.

Step 4: Insoluble phases

The residue from step 3 was gently heated with a mixture of 10 ml concentrated nitric acid and 8 ml perchloric acid for 24 h, and then shaken for 16 h at room temperature. The mixture was centrifuged at 10,000 rpm for 10 min to separate the residue. The supernatant solution was diluted by 0.1 M nitric acid to quantify by ICP-MS. Most insoluble phases decomposed in this step are silicates and sulfides.

Step 5: Residual phases (silicates resistant to the above reagents)

The residue from the previous steps was decomposed by alkaline fusion, and the solution was analyzed with 0.1 M HNO_3.

Quantification

After each step, major (Na, K, Ca, Mg, Al, Fe, and Mn) and toxic trace element (B, Cr, As, Pb, Cd, and Se) concentrations in the solution were analyzed by ICP-MS as described in section 3.2. The obtained results were expressed as the weight of leached elements from the powdered sediments (mg/kg, ppm). However, the B, As, and Pb concentrations of leachate after step 1 procedure were directly used for comparison with those of leachate by SBLT (mg/L), as following described in section 5.2.

3.4 Simple batch leaching test (SBLT)

Simple batch leaching tests were performed according to Japanese notification no. 46 (Japanese Ministry of Environment 1991). This test is required by Japanese law to evaluate the groundwater contamination risk from the use of excavated surplus soil.

Wet sediment samples were air-dried at room temperature for several days, then sieved to remove >2 mm (gravel) size fractions. A 3 g aliquot of the bulk sample was placed in a 50 ml plastic centrifuge tube with 30 ml water, of which pH was adjusted to 5.8–6.3 with hydrochloric acid and shaken horizontally for 6 h at 200 rpm. The solids were then collected by centrifugation at 3,000 rpm for 20 min, and the supernatant solution was decanted and passed through 0.45 and 0.1 μm membrane filters (A045A047A and A010A047A, respectively; Advantec Toyo, Japan). The former filtration procedure was performed according to Japanese notification no. 46, and the latter to evaluate the influence of

suspended particles passing through the 0.45 μm filter. In this study, both toxic and major element concentrations in the leached solutions were quantified to estimate the host phases and chemical forms of the toxic elements. Major (Na, K, Ca, Mg, Al, Fe, and Mn) and toxic trace elements (B, Cr, As, Pb, Cd, and Se) in the leachates were measured by ICP-MS as detailed in section 3.2. Anion concentrations (F^-, Cl^-, Br^-, and SO_4^{2-}) in the leached solutions were measured by ion chromatography (IC1200, Dionex) after filtration of the leached solutions (without added nitric acid) through a 0.2 μm membrane filter. The obtained results were expressed as the weight of leached elements in the leachates (mg/L) according to Japanese notification no. 46 (Japanese Ministry of Environment 1991).

4. Results

4.1 Lithology

Figure 2 summarizes the lithology of the sediment core, including the entire thickness of Ma13 (6-19 m depth), and shows the depths and physical properties (particle size distribution, water content, and LOI) of the 19 sediment samples studied herein (T-1 to T-19).

Sands were abundant above and below the clay layer, indicating changing depositional conditions during transgressive and regressive sea-level changes associated with Holocene climatic changes. Sediment water content decreased with increasing sand fraction and decreasing LOI. Silt and sand fractions were 59–67% and 15–28%, respectively, in the topmost sediments sampled (5.5–7.0 m depth). The silt fraction was similar (62–77%) at 7.0–10.4 m depth, but the sand fraction decreased to 2.5–5.2%. Sand pipes and common shells at 9–10 m depth indicate thriving biological activity. These uppermost sedimentary facies indicate a shallow brackish inner-bay coastal depositional environment during a regressive period. The middle part of Ma13 (11–16 m depth) was silty clay with fragile shell fragments and negligible sand fractions. The most homogeneous clay sediment in the core was observed at 12–13 m depth, suggesting the deepest water depositional environment (i.e., peak sea-level transgression). The maximum paleo-water depth in this study area has not been clarified, though it should have been about 15 m below sea-level based on estimations in coastal plains near the study site: the water depth at Suminoe (12 km SW of the study area) was 15 m during ca. 6,000–5,600 cal BP (Yasuhara et al. 2002), and that at Kitatsumori (6 km SW of the study area) was deeper than 15 m during ca. 5,500-5,000 cal BP (Masuda et al. 2002). Below 16 m depth, the sand fraction increased with increasing depth, reaching maximum sand fractions of >50% at 20 and 22 m depth. Based on the theory of sequence stratigraphy (e.g., Vail et al. 1991), these sand-dominated sediments are interpreted as a ravinement surface, i.e., relatively coarse and heterogeneous sediments formed by seafloor erosion during dramatic rises in sea level. Therefore, in this core, typical marine clays were observed at <20 m depth, and the sediments at 20–23.5 m depth were deposited during large sea-level fluctuations at the beginning of a transgression period.

We observed a concentration of volcanic glass at 19 m depth (just above the ravinement surface) with diffuse boundaries, suggesting bioturbation. Volcanic glass particles accounted for 19% of the sediment (among 100 counted sediment grains) at this depth. The refractive indices of these glass fragments indicate that they belong to the K-Ah (Kikai-Akahoya) tephra, which was erupted from Kikai Caldera (Kagoshima Prefecture) 7,300 years ago and is widely observed in the Japan Islands (Machida and Arai 2003). Thus, deposition of Ma13 in seawater of stable depth started around 7,000 years ago at this site, consistent with previous results (Masuda et al. 2002).

4.2 Bulk mineralogy and chemistry

XRD analyses revealed the mineralogy of the sediments to be quartz, feldspar, amphibole, pyrite, micas, chlorite, kaolinite, and smectite. XRD intensities of quartz and feldspar (Fig. 3) were positively correlated with sand fraction and negatively correlated with LOI and water content (Fig. 2). SiO_2 concentrations ranged from 64 to 76 wt% and varied with sand fraction and quartz and feldspar XRD intensities (Fig. 3). These results indicate that the sand fraction mainly comprised quartz and feldspar.

The concentrations of Al_2O_3 (12–18 wt%), Fe_2O_3 (2.8–6.1 wt%), MgO (0.8–2.2 wt%), and TiO_2 (0.39–0.76 wt%) varied similarly to LOI and opposite to SiO_2 concentration (Figs. 2 and 3). CaO concentration varied independently from the other major elements, probably due to contamination by biogenic carbonates such as shells and calcareous nanofossils. Na_2O (1.9–2.8 wt%) and K_2O concentrations (2.6–3.0 wt%) slightly decreased and increased with depth, respectively, suggesting an ion-exchange reaction between porewater and clay minerals.

Bulk B (25–75 ppm), Cr (25–75 ppm), and Pb (18–28 ppm) concentrations varied similarly to LOI, water content, and clay fraction (Figs. 2, 3). Bulk As concentrations (5–12 ppm) varied similarly to the above three elements, but with a maximum concentration at 9–10 m depth, where the silt fraction was the greatest. Furthermore, the trends of bulk As concentrations with depth were similar to that of Fe_2O_3 (Fig. 3), indicating that As was originated from iron minerals such as pyrite or Fe-oxyhydroxides/oxides. Bulk Cd and Se contents were <1 ppm; it was impossible to observe clear patterns related to the mineralogy or chemical composition of the sediments.

4.3 SCEE

The concentrations of the toxic elements B, As, Pb, and Cr extracted during the SCEE are shown in Figure 4. The total SCEE concentrations (i.e., the elemental concentrations summed over all extraction steps) accounted for more than 70, 90, 80, and 95% of the bulk B, As, Pb, and Cr concentrations, respectively. Immobile (i.e., insoluble and residual) phases were the most dominant host phases of these four elements.

B concentrations in insoluble and residual phases were 11–26 and 4–18 ppm, respectively, with the highest concentrations in the middle of Ma13. The concentration of acid-soluble B (3–15 ppm) was high among the mobile phases, with the highest concentration observed in the middle of Ma13 at 12–13 m depth, where the most homogeneous clay sediment was observed. B concentrations in acid-soluble and insoluble phases increased with increasing bulk B concentration (Fig. 5a). The acid-soluble B concentration also increased with increasing K and Na concentrations (Fig. 5b). K and Na are easily fixed within clay minerals (Buatier et al. 1992; Freed and Peacor 1992; Hover and Peacor 1999), and such ion-exchangeable cations are extracted as the acid-soluble phase in this procedure. Therefore, the positive correlations between acid-soluble B, K, and Na (Fig., 5b) imply that the acid-soluble B was desorbed from clay minerals.

Arsenic was most abundant in the insoluble phase (67–87% of the total As extracted); insoluble As concentrations ranged from 3.0 to 9.4 ppm, with the highest concentration occurring at 9–10 m depth. Insoluble As was strongly and positively correlated with bulk As (Fig. 5c) and positively correlated with insoluble Fe (Fig. 5d), suggesting that most insoluble As was fixed in sulfide minerals. Oxidizable As concentrations accounted for approximately 8–24% of the total As extracted, and they were higher in the upper part of Ma13 (1.3–2.1 ppm at 5.5–10 m depth) and the sediments underlying Ma13 (1.1–1.5 ppm at 20–21 and 23 m depths) than in the middle to lower parts of Ma13 (0.7–0.9

ppm at 11–19 m depth). Similar to the maximum insoluble As concentration, the maximum oxidizable As concentration (2.1 ppm) occurred at 9–10 m depth. Acid-soluble and reducible As were negligible compared to the oxidizable and insoluble concentrations.

Immobile Pb accounted for 70–90% of the total Pb extracted. The trend of insoluble Pb was similar to that of bulk Pb, with maximum concentrations at 12–15 m depth. Acid-soluble, reducible, and oxidizable Pb concentrations were higher in the upper and the lowermost parts of Ma13 (5.5–9 and 19 m depths) and the sediments underlying Ma13 (20–23 m depth) than in the middle to lower parts of Ma13 (10–18 m depth), except at 16 m depth, where the acid-soluble Pb concentration was the highest.

The concentrations of acid-soluble, reducible, and oxidizable Cr were relatively constant with depth, and much lower than the insoluble Cr concentrations, which slightly increased in the middle of Ma13.

4.4 SBLT

Figure 6 shows the results of the SBLT, i.e., the variations of major and toxic element concentrations and pH of leachates in relation to the sampling depth; the analytical results of solutions filtered to 0.1 μm are also compared to those of solutions filtered, per regulation, to 0.45 μm (Fig. 6b, c). The concentrations of Na, K, Ca, Mg, Mn, B, As, Cd, and Se in solutions filtered through the 0.45 and 0.1 μm filters are mostly the same, indicating that these elements were mostly dissolved in solution. On the other hand, the concentrations of Al (0.1–3.1 mg/L), Fe (0.06–0.08 mg/L), Pb (<0.006 mg/L), and Cr (<0.007 mg/L) in the 0.45 μm-filtered solutions were higher than those in the 0.1 μm-filtered solutions (Al: <0.2 mg/L, Fe: 0.01–0.08 mg/L, Cr: 0.002–0.004 mg/L, and Pb: not detected) at 6–9, 16, and 21–22 m depth. The concentration of Al at 13–14 m depth was also higher in the 0.45 μm-filtered solution.

Na, K, Cl^-, and Br^- concentrations produced arcuate trends with the lowest concentrations at the top and bottom of the studied section, and maximum concentrations at 12–13 m depth, in the middle of Ma13 (Fig. 6a, b). The Cl^- and Br^- concentrations were strongly and positively correlated (Fig. 7a). These halogens originate in seawater, and indeed, their maximum concentrations were observed in the deepest water interglacial sedimentation facies. Na and K concentrations were above typical seawater values (Fig. 7b, c), suggesting that they were added by mineral dissolution and/or ion-exchange reactions with clay minerals during the leaching test. The trends of K and Mg concentrations with depth were similar to that of SO_4^{2-} (i.e., having multiple maxima within Ma13). pH values were consistently between 7.0 and 7.5, but decreased to 5.2 in the bottom-most sediment analyzed.

F^- concentrations throughout most of Ma13 (up to 1.5 mg/L) exceeded the upper limit of Japanese regulations (0.8 mg/L), whereas other toxic elements were below regulation limits except for two samples: As (regulation value 0.01 mg/L) and B (0.1 mg/L) were at their regulation values at 9 and 11–12 m depth, respectively. The maximum B concentration (12 m depth) occurred where the Cl^- concentration was highest (290 ppm), and the B/Cl^- ratios were well above the seawater-freshwater mixing line (SW in Fig. 7d). Pb was only detected in the 0.45 μm-filtered solutions at 6–9, 16, and 21–22 m depth (maximum 0.006 mg/L at 9 m depth). The maximum bulk Cr concentration was lower than the regulation value (0.01 mg/L when present as a hexavalent ion). Arsenic concentrations were high at 6–9 and 16–19 m depth, parts of Ma13 deposited during regression and transgression periods, respectively. Cd concentrations were very close to the detection limit (0.05 μg/L). Se concentrations were generally low (<0.002 mg/L), but were slightly higher in the uppermost parts of Ma13.

5. Discussion

5.1 Factors controlling the dissolved concentrations of toxic elements

The "Amendment to the Soil Contamination Countermeasures Act" of Japan has streamlined the regulation of contaminated soils since 2017, when naturally contaminated excavated surplus soil was permitted for reuse. As noted above, the groundwater pollution risk of excavated surplus soils is legally evaluated based on the water-soluble fractions extracted by the SBLT. However, because this test does not account for the redox-dependent mobilities of toxic elements in the environment, it is important to specify the host phases and factors controlling the solubilities of naturally derived toxic elements. Here, we discuss the factors controlling the mobilities of B, As, and Pb.

In the SBLT, about 10% of the bulk B was water-soluble. The SCEE indicated that B was mainly hosted in acid-soluble and insoluble phases, which occur in relatively high proportions in clay-rich sediments. B is adsorbed predominantly on clay minerals (Williams et al. 2001), and strong positive correlations are observed between clay fractions and adsorbed B concentrations (Goldberg and Glaubig 1986). Water-soluble B concentrations were clearly high in the studied sediments with high proportions of silt and smaller size fractions (Figs. 2, 3, and 6). The highest water-soluble B concentration was observed at 12–13 m depth, where the highest Cl^-, Br^-, Na, and K concentrations were also observed. Thus, this highly mobile B is likely derived from seawater, in which the B concentration is typically 4.5 ppm, 450 times higher than the average value of stream waters (Faure 1998). In the studied sediments, B was adsorbed onto clay minerals such as chlorite, kaolinite, smectite, and micas (as detected by XRD analysis). Adsorbed B is easily desorbed from clay particles under the pH conditions of the SBLT solutions (mostly 7.0–7.5). At such pH conditions, B exists as the neutral oxyhydroxide $B(OH)_3$ (Choi and Chen 1979), which is incorporated along with water molecules in the interlayer of expandable smectite minerals (Williams and Herving 2005; Williams et al. 2007; Osawa et al. 2010). Thus, in the SBLT, B should have been extracted as an acid-soluble phase along with other ion-exchangeable cations such as Na and K (Fig. 5b).

Bulk As concentrations were within the ranges reported for present-day marine clays globally (3–15 ppm, Smedley and Kinniburgh 2002), in seabed sediments of Osaka Bay (3–15 ppm, n = 9, Geological Survey of Japan, AIST 2018; 5–13 ppm, n = 15, Osaka Prefecture Government 2018), and in Ma13 (6–26 ppm, Mitamura and Masuda 1998), and As was mostly present as oxidizable and insoluble phases. Among the insoluble phases, sulfide minerals are an important source of As. The primary As-bearing sulfides form in association with magmatism and related hydrothermal activities (e.g. Matschullat 2000; Masuda 2018), though diagenetic sulfide minerals can also be important sources of As. In particular, pyrite commonly found in sedimentary formations contains >2% As (e.g., Savage et al. 2000; Akai et al. 2004). Since the studied sediments contained pyrite at a level detectable by XRD analysis (i.e., on the order of a percent), a considerable amount of As must be incorporated into pyrite during diagenesis in Osaka Bay.

The maximum concentration of insoluble As was observed at 9–10 m depth, consistent with the trend of bulk As. Estuarine sediments from the southwestern Osaka Plain (Suminoe region), similar to our sediments at 9–10 m depth, were plausibly deposited at <10 m water depth (Yasuhara et al. 2002), where benthic organisms have high production volumes (Nixon 1988; Yamaguchi and Montani 2002). Generally, marine plants and algae easily accumulate inorganic As from seawater and partly transform it into organic forms in sediments (Francesconi and Edmonds 1996; Neff 2002). The concentrations of oxidizable (organic) As were also relatively high in the sediments at the same depth, implying As

accumulation by marine biological processes. Biologically promoted reducing environments occur in sediments associated with the decomposition of organic matter. Authigenic framboidal pyrite is commonly formed at ambient temperatures closely associated with activity of sulfate reducing bacteria (e.g. Kohn et al 1998; Popa et al 2004; Mozer 2010). Although it is difficult to fully explain the relationship of As and sulfide minerals observed herein, the insoluble As may have been partially fixed in authigenic pyrite under a biologically promoted reducing environment, especially at 9–10 m depth in the core.

Water-soluble As concentrations extracted by the SBLT were relatively high in the sediments at 6–9 and 16–19 m depth. Those sediments were sandy silts with shells and bioturbations, suggesting their deposition in a shallow inner-bay environment during regression and transgression periods. The sand fraction gradually decreased from 19 to 3% and increased from 3 to 30% with increasing depth in the 6–9 and 16–19 m depth intervals, respectively. These sandy silt sediments are the uppermost and lowermost sediments of Ma13, and are in contact with adjacent coarse sediment layers that act as groundwater aquifers. Therefore, As continuously released via oxidation-decomposition reactions of oxidizable and/or insoluble As phases in flowing groundwaters must have been adsorbed onto clay particles and/or other mineral surfaces.

The concentrations of water-soluble Pb in the 0.45 μm-filtered solutions were clearly higher than those in the 0.1 μm-filtered solutions and produced similar trends to those of Al and Fe (i.e., generally low concentrations with a prominent peak, Fig. 6), suggesting that colloidal particles passed through the 0.45 μm filter with the adsorbed Pb. Fe- and Al-hydroxides are known to combine with metal ions as surface complexes. For example, Pb^{2+} can be adsorbed onto the Fe-hydroxide surface by the following reaction (Wada 2008):

$$2\text{Fe-OH} + Pb^{2+} = (\text{Fe-O})_2\text{Pb} + 2H^{+}.$$

The ability of Pb^{2+} to bond to Fe- and/or Al-hydroxides decreases with decreasing pH (McGarvey et al. 1999). Thus, the Pb^{2+} was dissolved from surface complexes in the diluted nitric acid solution prepared for ICP-MS analyses. Importantly, these results confirm previous reports that the 0.45 μm filter is not sufficient to completely remove suspended particles, which affects evaluations of the mobility of certain toxic elements such as Pb (e.g., Yasutaka et al. 2017; Imoto et al. 2018; Ito et al. 2018).

5.2 Application to effective risk assessments of excavated surplus soils

For effective and realistic risk assessments of the reuse of excavated surplus soils, the relative index of metal mobility (mobility factor, MF) has been defined as the ratio of the sum of water-extractable, ion-exchangeable, and acid-soluble metal concentrations to the bulk metal concentration (Salbu et al. 1998; Narwal et al 1999; Kabala and Singh 2001; Kanjo et al. 2008). Here, because toxic elements in water-extractable and ion-exchangeable phases were extracted with acid-soluble phases in step 1 of the SCEE, we report MFs as the ratios of toxic element concentrations in acid-soluble phases to their bulk concentrations. The calculated MFs were 12–27% for B, <0.8% for As, and 1–12% for Pb. These values were also expressed as concentrations in the acid-soluble leaching solutions (mg/L), which reacted under the same ratio of liquid (L) (ml) to sediment (S) (g) as SBLT (L/S = 10), for comparison with water-soluble concentrations (Fig. 8). The acid-soluble concentrations of B, As, and Pb were 0.27–1.54, <0.008, and 0.02–0.32 mg/L, respectively, i.e., 2.6, 7, and >40 times their respective water-soluble concentrations (Fig. 8). These results suggest that the long-term risk of groundwater contamination from the reuse of excavated surplus soils is underestimated by the

regulation (0.45 μm filter) SBLT. For Pb specifically, the maximum recalculated concentration in the leaching solutions (0.32 mg/L) is 32 times the regulatory limit (0.01 mg/L), although the concentrations of water-soluble Pb were negligible when colloidal particles were filtered out (0.1 μm filter).

Leaching of B, As, and Pb from the analyzed marine clay sediments must be accelerated in oxic aqueous environments. For example, As dissolution accompanies the oxidation of pyrite with decreasing pH described by the reaction:

$$2FeS_2 + 7O_2 + 2H_2O \rightarrow 2Fe^{2+} + 4SO_4^{2-} + 4H^+.$$

This reaction can also accelerate the leaching of B and Pb from sediments. This reaction is one of the most realistic mechanisms for multiple toxic-element groundwater pollution resulting from the reuse of marine sediment-derived excavated surplus soils.

6. Conclusions

Holocene marine clay sediments in shallow alluvial coastal basins represent a contamination risk if exposed to environmental conditions differing from their *in-situ* underground conditions. Thus, excavated soils containing such clay sediments must be carefully treated when reused. In many cases, leaching of toxic elements from the soils may be accelerated by *in-situ* oxidation reactions. Therefore, excavated soils should be stored in reducing conditions, although they are generally exposed to aerobic conditions when reused in construction sites. For risk assessments of groundwater pollution resulting from the reuse of excavated soils, it is best to analyze soils more rigorously than required by regulations. Furthermore, it is necessary to continuously monitor any impacts on the surrounding environment after the reuse of excavated soils. From the point of view of reducing construction waste to achieve a sustainable geo-environment, our methods are more appropriate than those currently required to evaluate the risks of reusing extracted surplus soils, especially when considering long-term effects.

Acknowledgement

The authors thank N. Kitada and T. Fujiwara for sample treatments, and K. Okazaki for analytical assistance in the laboratory.

References

Akai J, Izumi K, Fukuhara H, Masuda H, Nakano H, Yoshimura T, Ohfuji H, Anawar H Md and Akai K (2004) Mineralogical and geomicrobiological investigations on groundwater arsenic enrichment in Bangladesh. Appl Geochem 19:215-230

Buatier MD, Peacor DR, O'Neil JR (1992) Smectite-illite transition in Barbados accretionary wedge sediments: TEM and AEM evidence for dissolution/crystallization at low temperature. Clay Clay Miner 40:65–80

Choi W-W, Chen KY (1979) Evaluation of boron removal by adsorption on solids. Environ Sci Technol 13:189–196

Danhara T, Yamashita T Iwano H, Kasuya M (1992) An improved system for measuring reflective index using the thermal immersion method. Quatern Intl 13/14:89–91

Faure G (1998) Principles and Applications of Geochemistry (Second Edition), Prentice Hall in Upper Saddle River, New Jersey, ISBN 0023364505

Francesconi KA, Edmonds JS (1996) Arsenic and Marine Organisms. Adv Inorg Chem 44:147–189

Freed RL, Peacor DR (1992) Diagenesis and the formation of authigenic illite-rich I/S crystals in Gulf Coast shales: TEM study of clay separates. J Sediment Petrol 62:220–234

Geological Survey of Japan (AIST) (2018) Geochemical Map of Sea and Land of Japan. https://gbank.gsj.jp/geochemmap/ocean/data/seadata.htm. Accessed 18 December 2018 (in Japanese)

Goldberg S, Glaubig RA (1986) Boron Adsorption on California Soils. Soil Sci Soc Am J, 50:1173–11176

Hover VC, Peacor DR (1999) Direct evidence for potassium uptake in smectite during early diagenesis of marine sediments and MORB: Balancing the global potassium budget. Clay Mineral Society Meeting Program and Abstracts, 36th Annual Meeting, Purdue University, West Lafayette, 50

Ichihara M (ed.) (1993) The Osaka Group, Sogen-sha, ISBN 4422220039 (in Japanese)

Imoto Y, Yasutaka T, Someya M, Higashino K (2018) Influence of solid-liquid separation method parameters employed in soil leaching tests on apparent metal concentration. Sci Total Environ 624:96–105

Ito H, Masuda H, Kusakabe M (2003) Some factors controlling arsenic concentrations of groundwater in the northern part of Osaka Prefecture. J Groundwat Hydrol 45(1):3–18 (In Japanese with English abstract)

Ito H, Masuda H, Oshima A (2018) Concentrations of the naturally-derived toxic elements and its geochemical characteristics of the alluvial marine clay layer of Osaka Plain, Japan. Proceedings of the 8th International Congress on Environmental Geotechnics 1:504–511

Japanese Geotechnical Society (2015) JGS 1221-2012 Method for obtaining soil samples using thin-walled tube sampler with fixed piston. Japanese Geotechnical Society Standards: Geotechnical and Geo-environmental Investigation Methods, Vol.1, Maruzen Publishing Co., Ltd., ISBN 978-4-88644-820-0

Japanese Industrial Standard Association (2009a) JIS A 1203 Test method for water content of soils. http://www.jisc.go.jp/app/jis/general/GnrJISSearch.html. Accessed 4 January 2019 (in Japanese)

Japanese Industrial Standard Association (2009b) JIS A 1204 Test method for particle size distribution of soils. http://www.jisc.go.jp/app/jis/general/GnrJISSearch.html. Accessed 4 January 2019 (in Japanese)

Japanese Industrial Standard Association (2009c) JIS A 1226 Test method for ignition loss of soils. http://www.jisc.go.jp/app/jis/general/GnrJISSearch.html. Accessed 4 January 2019 (in Japanese)

Japanese Ministry of the Environment (2003 a) Environmental Agency notifications no. 18 (Analytical methods of simple batch leaching test) https://www.env.go.jp/water/dojo/law/kokuji.html Accessed 25 February 2019 (in Japanese)

Japanese Ministry of the Environment (2003 b) Environmental Agency notifications no. 19 (Analytical methods of acid leaching test) https://www.env.go.jp/water/dojo/law/kokuji.html Accessed 25 February 2019 (in Japanese)

Japanese Ministry of the Environment (1991) Environmental Agency notifications no. 46 (Environmental standards relating to contamination of soil) http://www.env.go.jp/kijun/dojou.html Accessed 25 February 2019 (in Japanese)

Japanese Ministry of the Environment (2017 a) Amendment to the Soil Contamination Countermeasures Act http://elaws.e-gov.go.jp/search/elawsSearch/elaws_search/lsg0500/detail?lawId=414AC0000000053 Accessed 25 February 2019 (in Japanese)

Japanese Ministry of the Environment (2017 b) Enforcement Notice of the Soil Contamination Countermeasures Act, no. 1703313 https://www.env.go.jp/water/dojo/law/kaisei2009/no_100305002.pdf Accessed 25 February 2019 (in Japanese)

Japanese Ministry of the Environment (2017 c) Enforcement Regulation of the Soil Contamination Countermeasures Act, Ordinance no. 29 of Ministry of the Environment http://elaws.e-gov.go.jp/search/elawsSearch/elaws_search/lsg0500/detail?lawId=414M60001000029 Accessed 25 February 2019 (in Japanese)

KG-NET: Kansai Geo-informatics Network (2007) Shi-Kansai Jiban -From Osaka Plain to Osaka Bay Area- (in Japanese)

Kabala C, Singh BR (2001) Fractionation and mobility of copper, lead, zinc in soil profiles in the vicinity of a copper smelter. J Environ Qual 30:485–492

Kanjo Y, Nouri M, Kase T (2008) Application of Modified BCR Sequential Extraction Procedure for Evaluation of Heavy Metal Leaching in Contaminated Soil. J Jap Soc Civil Engin G64(4):304–313 (In Japanese with English abstract)

Kohn MJ, Riciputi LR, Stakes D, Orange DL (1998) Sulfur isotope variability in biogenic pyrite: Reflections of heterogeous bacterial colonization ? Ame Mineral 83: 1454-1468

Machida H, Arai F (2003) Atlas of tephra in and around Japan (revised edition). University of Tokyo Press, ISBN 4-13-060745-6 (in Japanese)

MacLean LC, Tyliszczak T, Gilbert PU, Zhou D, Pray TJ, Onstott TC, Southam G (2008) A high-resolution chemical and structural study of framboidal pyrite formed within a low-temperature bacterial biofilm. Geobiology 6: 471-480

Masuda F, Irizuki T, Fujiwara O, Miyahara B, Yoshikawa S (2002) A Holocene sea-level curve constructed from a single core at Osaka, Japan (A preliminary note). Mem Fac Sci Kyoto Univ, Ser Geol Mineral 59(1):1–8

Masuda H (2018) Arsenic cycling in the Earth's crust and hydrosphere: interaction between naturally occurring arsenic and human activities. Prog Earth Planet Sci, 5: 68

Matschullat J (2000) Arsenic in geosphere – a review. Sci Total Environ 249: 297-312

McGarvey GB, Ross KJ, McDougall TE, Turner CW (1999) Lead Corrosion and Transport in Simulated Secondary Feedwater. Atomic Energy of Canada Limited, ISSN 0067-0367. https://inis.iaea.org/collection/NCLCollectionStore/_Public/31/030/31030413.pdf. Accessed 9 January 2019

Mitamura M, Masuda H (1998) Arsenic content of drilling cores in Osaka and its surrounding area. Proceedings of the 8th Symposium on Geo-Environments and Geo-Technics: 85–88 (In Japanese with English abstract)

Mozer A (2010) Authigenic pyrite framboids in sedimentary facies of the Mount Wawel Formation (Eocene), King George Island, West Antarctica. Polish Polar Research 31 (3): 255-272

Narwal RP, Singh BR, Salbu B (1999) Association of cadmium, zinc, copper, and nickel with components in naturally heavy metal rich soils studied by parallel and sequential extractions. Commun Soil Sci Plan Anal 30:1209–1230

Neff JM (2002) Chapter 3: Arsenic in the ocean. In: Bioaccumulation in Marine Organisms: Effect of Contaminants from Oil well produced water:57–78, Elsevier Science, eBook ISBN: 9780080527840

Nixon SW (1988) Physical energy inputs and the comparative ecolgy of lake and marine ecosystems. Limnol Oceanorg 33:1005–1025

Osaka Prefecture Government (2018) Results of sea bottom sediments investigation in Osaka Bay, 2012 http://www.pref.osaka.lg.jp/kankyohozen/osaka-wan/teisitsu.html. Accessed 18 December 2018 (in Japanese)

Osawa S, Amita M, Yamada M, Mishima T, Kazahaya K (2010) Geochemical Features and Genetic Process of Hot-spring Waters Discharged from Deep Hot-spring Wells in the Miyazaki Plain, Kyushu Island, Japan: Diagenetic Dehydrated Fluid as a Source Fluid of Hot-spring Water, J. Hot Spring Sci 59:295–319 (In Japanese with English abstract)

Popa R, Kinkle BK, Badescu A (2004) Pyrite framboids as biomarkers for iron-sulfur systems. Geomicrobiol J 21: 193-206

Public Works Research Institute et al (eds) (2015) Handbook of excavated surplus soils containing naturally-derived heavy metals. Taisei Shuppan, ISBN 978-4-8028-3193-2 (in Japanese)

Salbu B, Krekling T, Oughton DH (1998) Characterization of radioactive particles in the environment. Analyst 123:843–849

Savage KS, Tingle TN, O'Day PA, Waychunas GA, Bird DK (2000) Arsenic speciation in pyrite and secondary weathering phases, Mother Lode Gold District, Tuolumne County, California. Appl Geochem 15:1219–1244

Smedley PL, Kinniburg DG (2002) A review of the source, behavior and distribution of arsenic in natural waters. Appl Geochem 17:517–568

Thomas RP, Ure AM, Davison CM, Littlejohn D, Rauret G, Rubio R, Lopez-Sanches JF (1994) Three-stage sequential extraction procedure for the determination of metals in river sediments. Analytica Chemica Acta 286:423–429

Vail PR, Audemard F, Boeman SA, Eisner PN, Perez-Cruz C (1991) The stratigraphic signatures of tectonics, eustasy and sedimentology - an overview. In: Einsele G, Ricken W and Seilacher A (eds.) Cycles and events in stratigraphy 6: 617–659, Springer-Verlag, Berlin, ISBN 978-0387527840

Wada S (2008) Clays and Soil Pollution. Nendokagaku (Clay Science) 47(3):185–195 (in Japanese)

Wang N, Ouyang T, Yun SJ, Iwashima K (1997) The chemical forms of As in soils of Chiba Prefecture. Kankyo to Sokuteigijutu (Environment and Measurement Techniques) 24:7–11 (in Japanese)

Williams LB, Hervig RL (2005) Lithium and boron isotopes in illite-smectite: The importance of crystal size. Geochim Cosmochim Acta 69:5705–5716

Williams LB, Hervig RL, Holloway JR, Hutcheon I (2001) Boron isotope geochemistry during diagenesis: Part 1. Experimental determination of fractionation during illitization of smectite. Geochim Cosmochim Acta 65:1769–1782

Williams LB, Turner A, Hervig RL (2007) Intercrystalline boron isotope partitioning in illite-smectite: Testing the geothermometer. Am Miner 92:1958‑1965

Yamaguchi H, Montani S (2002) Biological production in coastal seas with relation to benthic organisms. Jap J Limnol 63:241–248 (In Japanese with English abstract)

Yasuhara M, Irizuki T, Yoshikawa S, Nanayama F (2002) Holocene sea-level changes in Osaka Bay, western Japan: ostracode evidence in a drilling core from the southern Osaka Plain. Jour Geol Soc Japan 108 (10):633–643

Yasutaka T, Imoto Y, Kurosawa A, Someya M, Higashino K, Kalbe U, Sakanakura H (2017) Effects of colloidal particles on the results and reproducibility of batch leaching tests for heavy metal-contaminated soil. Soils Found 57:861–871

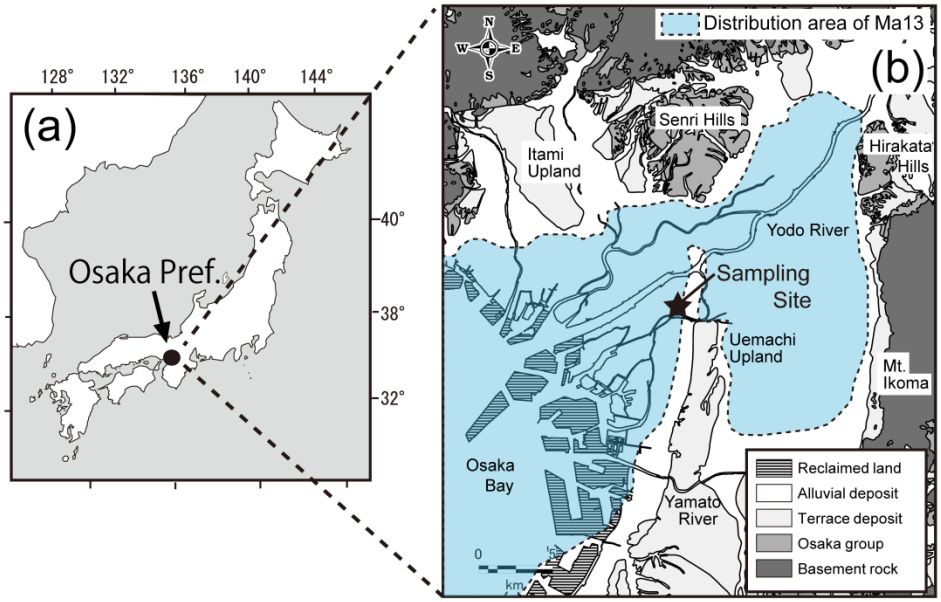

Fig. 1 Maps of the study site (a) Location of the Osaka Prefecture of Japan (b) Geological map (recompiled from Ichihara 1993), distribution area of Ma13 (based on KG-NET 2007) and the location of the sampling site

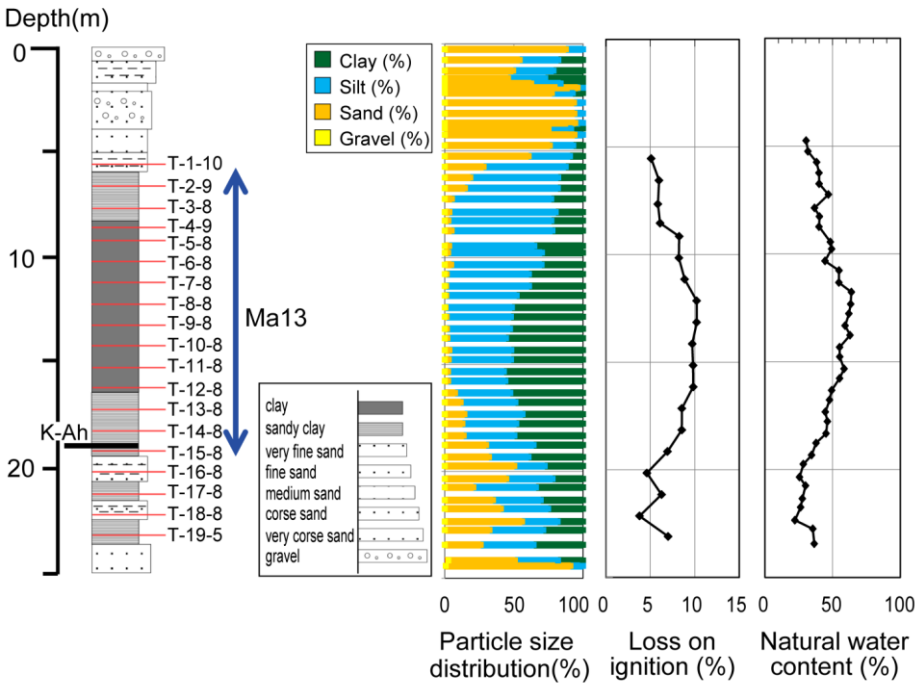

Fig. 2 Geological columnar section with the particle size distribution, loss on ignition, and natural water content

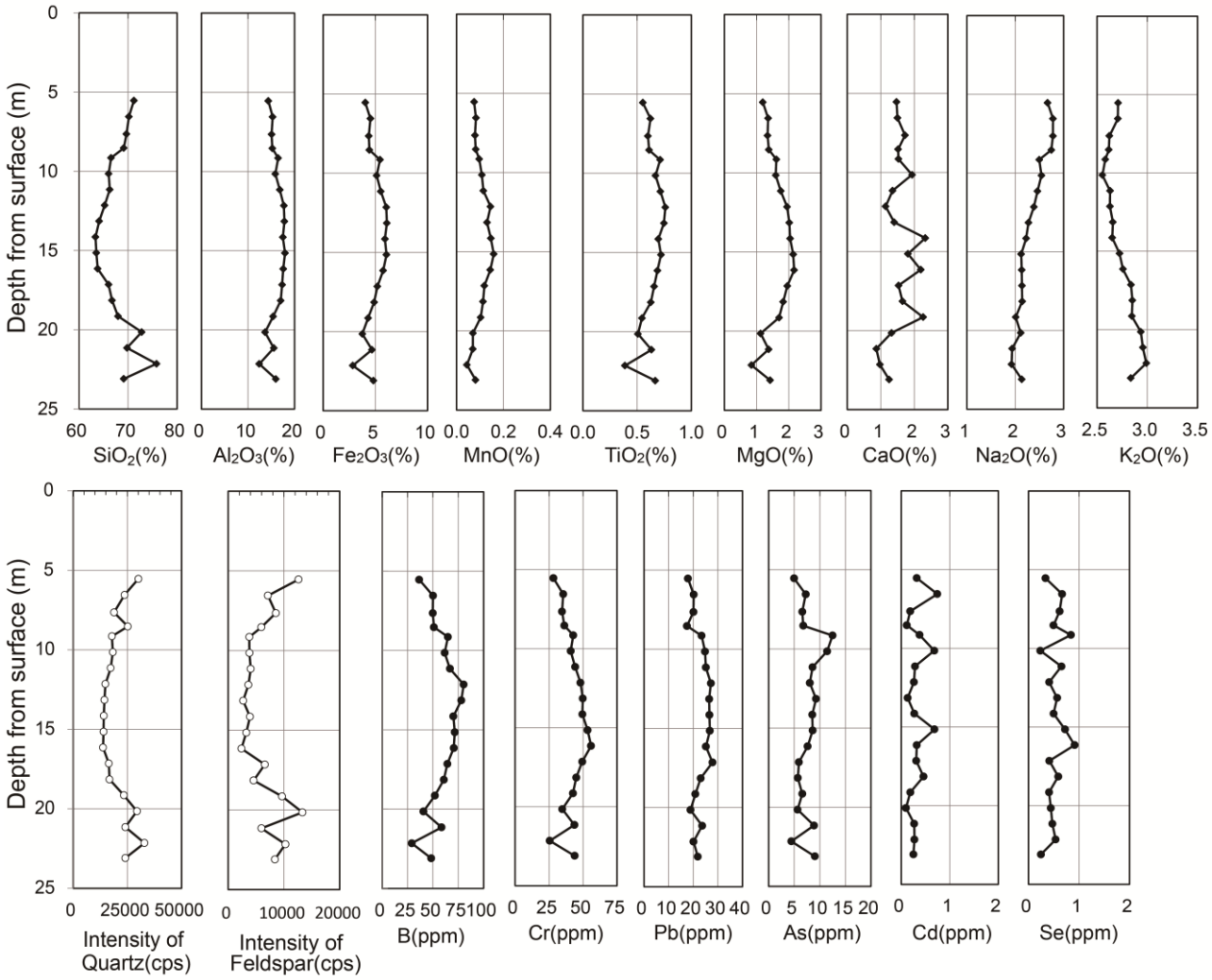

Fig. 3 Bulk concentrations of major and toxic elements with depth, and the intensities of the most intense diffraction peaks of quartz (d = 3.34 Å) and feldspar (d = 3.19-3.24 Å) of powder XRD

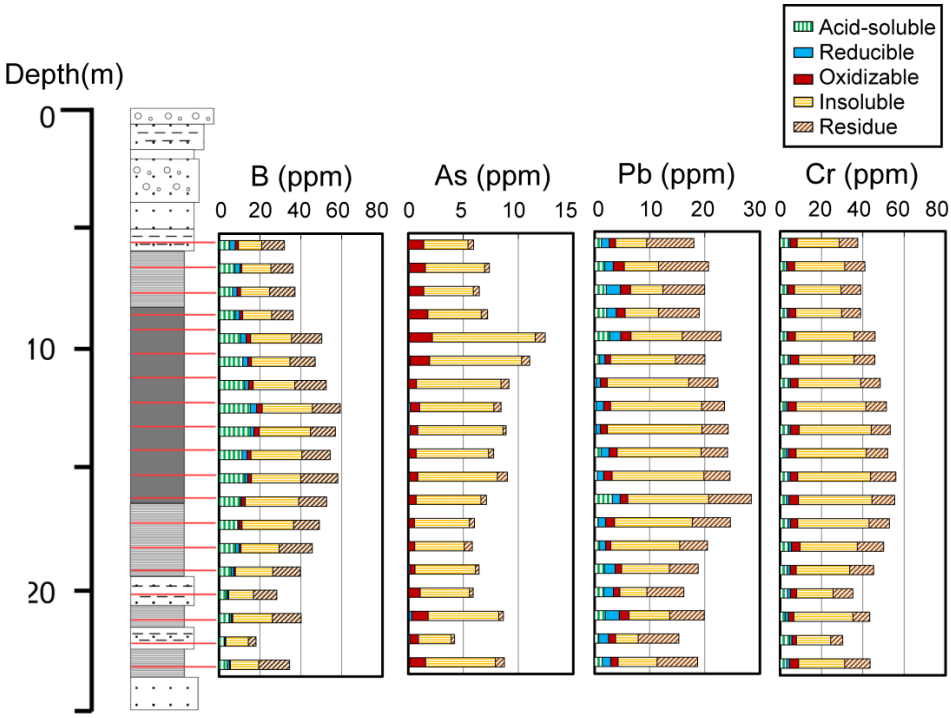

Fig. 4 Concentrations of B, As, Pb and Cr extracted by the SCEE (The legend of geological columnar section was shown in Fig. 2)

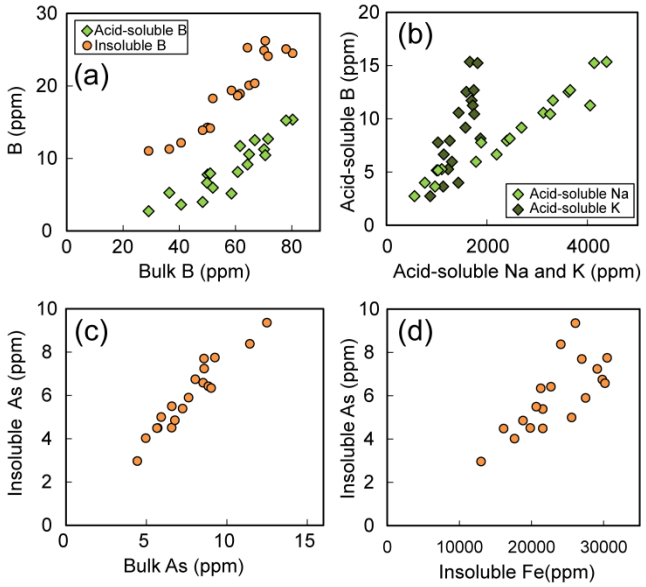

Fig. 5 Relationships between (a) bulk and acid soluble / insoluble concentrations of B, (b) acid soluble Na / K and B concentrations, (c) bulk and insoluble As concentrations, (d) insoluble Fe and As concentrations

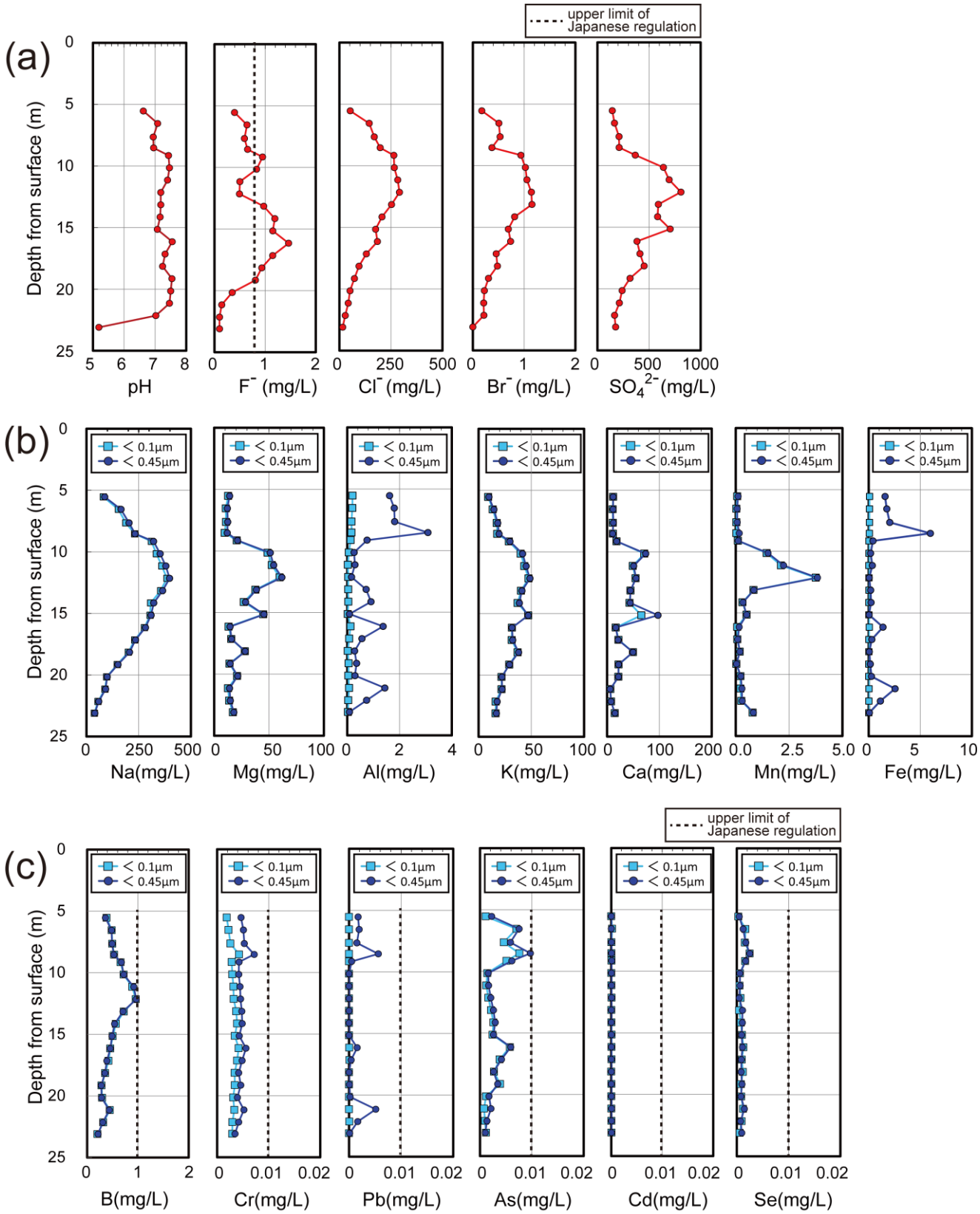

Fig. 6 Concentrations of major and toxic elements and pH values in the leachates treated by the SBLT (a) anion concentrations of <0.2 μm-filtered solutions, (b) cation concentrations of both <0.45 and <0.1 μm-filtered solutions, (c) toxic element concentrations of both <0.45 and <0.1 μm-filtered solutions (recompiled from Ito et al. 2018)

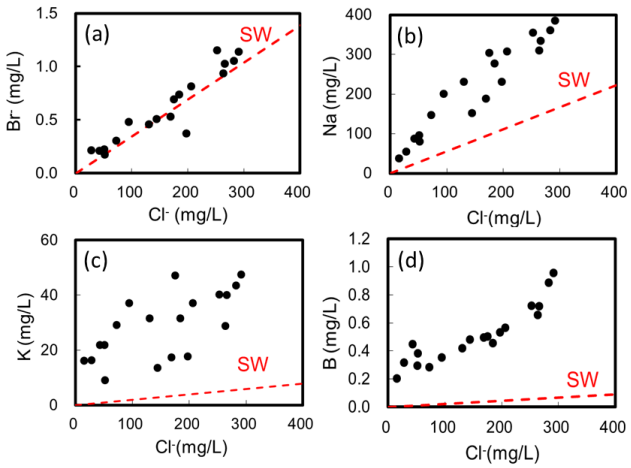

Fig. 7 Relationships between Cl^- and (a)Br^-, (b)Na, (c)K and (d)B concentrations (SW: seawater-freshwater mixing lines)

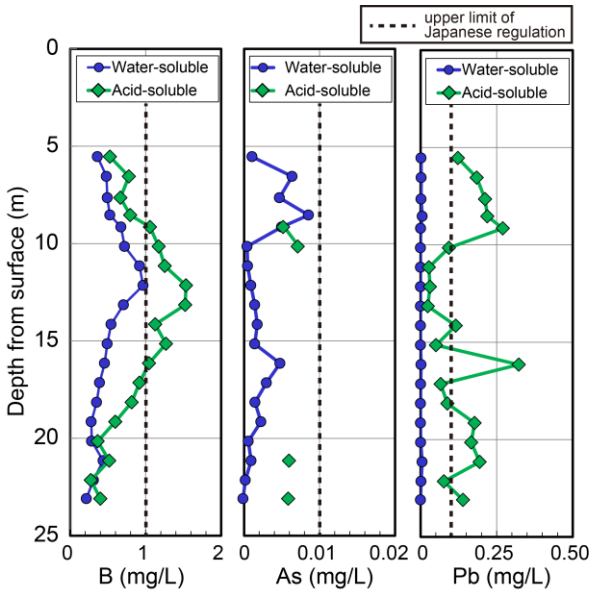

Fig. 8 Comparisons of water-soluble and acid-soluble concentrations of B, As, and Pb reacted under the same ration of liquid (L) (ml) to sediment (S) (g) (L/S = 10)